Proceedings of the
44th IEEE Conference on Decision and Control, and
the European Control Conference 2005
Seville, Spain, December 12-15, 2005

Modeling of an inkjet printhead for Iterative Learning Control using bilaterally coupled multiports

M.B. Groot Wassink* and O.H. Bosgra* and D.J. Rixen** and S.H. Koekebakker***

Abstract— **Modeling an inkjet printhead usually comprises a trade-off between high accuracy and small computational load. In face of the control purpose in mind, this paper presents a modeling strategy that breaks this boundary. For that purpose, an inkjet printhead is modeled as series connection of bilaterally coupled multiports using first principles only. By experimental validation, it is shown that the adopted model structure and parameters result in an accurate fit of the actual system. Next, the resulting model and the accompanying physical insight are used to improve the actuation of an inkjet printhead. The successful implementation of ILC based on the obtained model not only shows the model's applicability to control, but also provides new input pulses that enable higher jetting frequencies.**

I. INTRODUCTION

Inkjet technology is an important key-technology from an industrial point of view. Its ability to deposit various types of material on a substrate in certain patterns makes it a very versatile technology. Not surprisingly, applications of this technology cover a wide range from the traditional document printing to the manufacturing of electronics such as Flat Panel Displays (e.g. [1]), the production of organic electronics (e.g. [2]), and the use for rapid prototyping (e.g. [3]). Each specific field of application imposes its own performance requirements on the inkjet printhead. First, specifications in terms of timing, positioning, and volume have to be met. Often, these criteria are quite tight. Typically, one can think of an accuracy to be met in terms of fractions of microseconds, micrometers and picoliters. Second, requirements play a role concerning reproducibility in face of aging, material and ink variations, and the like. In the future, these performance criteria will become even tighter. The requirements for future applications motivate ongoing research into inkjet technology.

Modeling plays an essential role in the development of inkjet technology. For example, models can provide insight into a specific printhead design that is required for its further optimization. Also, they can be used for the synthesis of input wave forms or controllers, such as for Iterative Learning Control (ILC) ([11]). Though for the applications mentioned above a relatively simple yet accurate model suffices, modeling an inkjet printhead still is a challenging task given its complex nature. It comprises, among other things, fluid-structure interaction, acoustics, fluid-mechanics, free surface flow, and drop-formation. To deal with these phenomena, almost all modelers resort to the use of finite element packages and computational fluid dynamics (e.g. [4]). The use of these packages induce large computational time. Additionally, since various physical domains have to be coupled, usually it also comprises the use of staggered schemes (e.g. [7]). This further increases the computational load. The resulting models, though accurate, are not suitable for the application of control, e.g. ILC.

In this paper, a modeling strategy is presented that does not suffer from the aforementioned computational burden yet offers the required accuracy. Using first principle modeling only, an inkjet channel is modeled as a system of bilaterally coupled multiports. The basic concepts employed in this paper originate from the analysis of fluid transmission lines ([15], [16]). For the inkjet channel, these concepts are further elaborated and formulated within a multiport framework ([9], [14]). The coupling of these subsystems and their physical domains is achieved by the application of Redheffer's star product ([8]). Furthermore, by using the resulting model and the physical insight it provides, the actuation of an inkjet printhead is improved such that higher jetting frequencies can be attained. This is accomplished by the implementation of lifted ILC ([18], [19], [20]).

The paper is organized as follows. First, a system description is provided in Section II. Then, the theoretical modeling is discussed in Section III. In Section IV, the obtained model is validated using experimental results. Its applicability to ILC is demonstrated in Section V. Finally, Section VI presents the conclusions and gives an outlook on future work.

II. SYSTEM DESCRIPTION

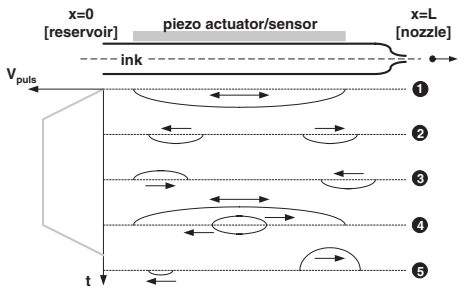

Fig. 1. A schematic view of an inkjet channel and its working principle

* M.B. Groot Wassink and O.H. Bosgra are with Delft Center for Systems and Control, Delft University of Technology, 2628 CD Delft, The Nederlands m.b.grootwassink@dcsc.tudelft.nl

** D.J. Rixen is with Delft University of Technology, 2628 CD Delft, The Netherlands

*** S.H. Koekebakker is with Océ-Technologies B.V., 5900 MA Venlo, The Netherlands

0-7803-9568-9/05/$20.00 ©2005 IEEE

A schematic view of a channel of an inkjet printhead is depicted in Fig. 1. It consists of a channel of several millimeters, a nozzle, and a piezo-actuator. Typically, around 75 nozzles per inch are integrated in an array that forms a printhead. To fire a droplet, a trapezoidal pulse is provided to the piezo actuator. Then, ideally, the following occurs. To start with, a negative pressure wave is generated in the channel by enlarging the volume in the channel (step 1). This pressure wave splits up and propagates in both directions (step 2). These pressure waves are reflected at the reservoir that acts as an open end and at the nozzle that acts as a closed end (step 3). Note that the pressure wave reflecting at the nozzle is not large enough to result in a droplet yet. Next, by decreasing the channel's volume to its original value a positive pressure wave is superposed on the reflected waves exactly when they are located in the middle of the channel (step 4). Consequently, the wave travelling towards the reservoir is cancelled whereas the wave travelling towards the nozzle is amplified such that it is large enough to result in a droplet (step 5). Typically, a printhead is operated at 10 kHz. It takes about 20 μs to fire a droplet and around 200 μs for the pressure waves to be completely damped. Most of the damping occurs in the nozzle of an ink channel.

According to [5], the piezo-actuator is concurrently used as sensor. Physically, it senses the force that results from the pressure distribution in the channel acting on the piezo's surface that borders the channel. This force creates a charge on the piezo unit. Since only changes in charge are measured, in fact the time derivative of the instantaneous present force is sensed. Furthermore, since the resulting voltage drop of this current over a resistance is measured, we have that a voltage is the eventual sensor signal. For the trapezoidal pulse used for actuation, a typical sensor signal is depicted in Fig. 9. The following remarks concerning this sensor signal are noteworthy. First, due to the integrating character of the sensor the resulting signal is an average of the pressure that is present in a channel. Second, since all the piezo's are connected to the same substrate, the actuation as well as sensing is influenced by structural cross-talk. Despite all these facts, the current sensor signal can be regarded as representative for the jetting process. Consequently, in this paper a model is derived that has the pulse sent to the piezo as input and has the described sensor signal as output. The accompanying measured transfer function will serve as validation for the twoport model.

During the derivation, it is assumed that a printhead behaves linearly. In [11], it was demonstrated that the non-linear effect of jetting a droplet is so small that from a control perspective the operation of a printhead indeed can be regarded as linear.

III. THEORETICAL MODELING

In this section, the theoretical modeling of an inkjet channel is discussed. To start with, the inkjet channel is divided into several subsystems that make up the complete model. Next, each subsystem is discussed shortly. Finally, the coupling of these subsystems is discussed and the resulting overall model is analyzed. Note that to obtain a model of a complete printhead, as many as appropriate channel models can be merged. This will be addressed in this section as well.

A. The model structure

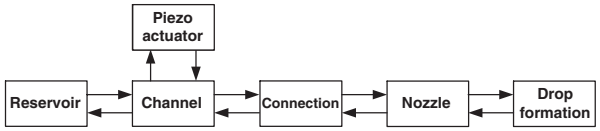

Fig. 2. A schematic overview of the twoport model of an inkjet channel

In Fig. 2, a schematic overview is given of the twoport model of the inkjet channel depicted in Fig. 1. This partition into subsystems is based on the specific design of the inkjet channel under consideration. To start with, the segment of the channel that is actuated by the piezo-actuator is called the channel block. It differs only from the connection block by the fact that the latter is not actuated. The reservoir forms the physical boundary of an inkjet channel and also forms the boundary of the model. As all these three blocks can be modeled using acoustics, they are referred to as acoustic path. The following two blocks, those of the nozzle and droplet formation, are modeled using the basic equations in fluid-mechanics. Together, they make up the fluidic path. The last block is that of the piezo-actuator. Note that a block representing the electrical part of the inkjet channel is omitted since it does not contribute significantly to the dynamics of the printhead. If required though, it can be incorporated straightforwardly.

B. The acoustic path

The acoustic path consists of the channel, connection, and reservoir. To start with, it is assumed that for these blocks a one dimensional approach can be used. This implies that only plane waves occur during operation of an inkjet channel. Flow3D simulations confirm the validity of this approach. Second, it is assumed that there is no mean flow and that only small perturbations occur. This is a valid assumption, since the volume that is jetted is so small that this is hardly noticeable as mean flow in the channel. Finally, the dissipation also is assumed to be negligible.

The modeling of the channel is treated first. To that purpose, we start with the conservation of mass and momentum for a channel with variable cross-section $A(x,t)$:

$$\frac{\partial A(x,t)\rho(x,t)}{\partial t} + \frac{\partial A(x,t)\rho(x,t)v(x,t)}{\partial x} = 0 \tag{1}$$

$$\frac{\partial A(x,t)\rho(x,t)v(x,t)}{\partial t} + \frac{\partial A(x,t)v^2(x,t)\rho(x,t)}{\partial x} + \frac{\partial A(x,t)p(x,t)}{\partial x} = 0 \tag{2}$$

Here, $v(x,t)$, $p(x,t)$, $A(x,t)$, and $\rho(x,t)$ are the velocity, pressure, channel cross-section, and density, respectively. (1) can be written as:

$$\frac{\partial A(x,t)\rho(x,t)}{\partial t} + A(x,t)\rho(x,t)\frac{\partial v(x,t)}{\partial x} + v(x,t)\frac{\partial A(x,t)\rho(x,t)}{\partial x} = 0 \tag{3}$$

and (2) as:

$$v(x,t)\frac{\partial A(x,t)\rho(x,t)}{\partial t} + A(x,t)\rho(x,t)\frac{\partial v(x,t)}{\partial t} + 2A(x,t)\rho(x,t)v(x,t)\frac{\partial v(x,t)}{\partial x} + v^2(x,t)\frac{\partial A(x,t)\rho(x,t)}{\partial x} + \frac{\partial A(x,t)p(x,t)}{\partial x} = 0 \tag{4}$$

Using the mass balance (3), (4) can be written as:

$$A(x,t)\rho(x,t)\frac{\partial v(x,t)}{\partial t} + A(x,t)\rho(x,t)v(x,t)\frac{\partial v(x,t)}{\partial x} + \frac{\partial A(x,t)p(x,t)}{\partial x} = 0 \tag{5}$$

Now, $A(x,t)v(x,t)$ is replaced by $\phi(x,t)$. Furthermore, it is assumed that the variations in density and pressure under adiabatic conditions are related through:

$$\frac{dp}{d\rho}|_{\text{adiabatic}} = c_w^2 \quad \rightarrow \quad \frac{d\rho}{dt} = \frac{1}{c_w^2}\frac{dp}{dt} \quad \text{and} \quad \frac{d\rho}{dx} = \frac{1}{c_w^2}\frac{dp}{dx} \tag{6}$$

where c_w is the wave propagation velocity. After the appropriate substitutions, both equations (1) and (5) are linearized. Consequently, the coefficients $v(x,t)$, $\frac{c_w^2\rho(x,t)}{A(x,t)}$, $\frac{A(x,t)}{\rho(x,t)}$, and $\frac{p(x,t)}{\rho(x,t)}$ are considered constant having the nominal values v, $\frac{c_w^2\rho}{A}$, $\frac{A}{\rho}$, and $\frac{p}{\rho}$, respectively. If the variables are from now assumed to represent deviations from their nominal value, the set of conservation laws can be written in vector form as:

$$\frac{\partial}{\partial t}\begin{bmatrix} p(x,t) \\ \phi(x,t) \end{bmatrix} + \begin{bmatrix} v & \frac{c_w^2\rho}{A} \\ \frac{A}{\rho} & v \end{bmatrix}\frac{\partial}{\partial x}\begin{bmatrix} p(x,t) \\ \phi(x,t) \end{bmatrix} = \begin{bmatrix} -\frac{c_w^2\rho}{A} \\ v \end{bmatrix}\frac{\partial}{\partial t}A(x,t) + \begin{bmatrix} 0 \\ v^2 - \frac{p}{\rho} \end{bmatrix}\frac{\partial}{\partial x}A(x,t) \tag{7}$$

The eigenvalues of matrix $\begin{bmatrix} v & \frac{c_w^2\rho}{A} \\ \frac{A}{\rho} & v \end{bmatrix}$ have the values $\lambda_{1,2} = v \pm c_w$. Its corresponding eigenvectors are:

$$m_1 = \begin{bmatrix} \frac{c_w\rho}{A} \\ 1 \end{bmatrix} \qquad m_2 = \begin{bmatrix} -\frac{c_w\rho}{A} \\ 1 \end{bmatrix} \tag{8}$$

If we now define:

$$\begin{bmatrix} z_1(x,t) \\ z_2(x,t) \end{bmatrix} = \begin{bmatrix} m_1 & m_2 \end{bmatrix}^{-1} = \begin{bmatrix} \frac{A}{2c_w\rho} & \frac{1}{2} \\ -\frac{A}{2c_w\rho} & \frac{1}{2} \end{bmatrix}\begin{bmatrix} p(x,t) \\ \phi(x,t) \end{bmatrix} \tag{9}$$

then (7) can be brought to the form:

$$\frac{\partial}{\partial t}\begin{bmatrix} z_1(x,t) \\ z_2(x,t) \end{bmatrix} + \begin{bmatrix} v+c_w & 0 \\ 0 & v-c_w \end{bmatrix}\frac{\partial}{\partial x}\begin{bmatrix} z_1(x,t) \\ z_2(x,t) \end{bmatrix} = \begin{bmatrix} \frac{v-c_w}{2} \\ \frac{v+c_w}{2} \end{bmatrix}\frac{\partial}{\partial t}A(x,t) + \begin{bmatrix} \frac{\rho v^2 - p}{2\rho} \\ \frac{\rho v^2 - p}{2\rho} \end{bmatrix}\frac{\partial}{\partial x}A(x,t) \tag{10}$$

Note that $z_1(x,t)$ and $z_2(x,t)$ have the physical dimension of flow. After application of the Laplace transform while assuming zero initial conditions and some reshuffling we obtain:

$$\frac{\partial}{\partial x}\begin{bmatrix} z_1(x,s) \\ z_2(x,s) \end{bmatrix} = \begin{bmatrix} -\frac{s}{c_w+v} & 0 \\ 0 & \frac{s}{c_w-v} \end{bmatrix}\begin{bmatrix} z_1(x,s) \\ z_2(x,s) \end{bmatrix} + \begin{bmatrix} \frac{-s(c_w-v)}{2(c_w+v)} \\ \frac{-s(c_w+v)}{2(c_w-v)} \end{bmatrix}A(x,s) + \begin{bmatrix} \frac{\rho v^2 - p}{2\rho(c_w+v)} \\ \frac{p-\rho v^2}{2\rho(c_w-v)} \end{bmatrix}\frac{\partial}{\partial x}A(x,s) \tag{11}$$

This renders the partial differential equation to an ordinary one that can be solved straightforwardly. Prior to that, the forcing function $A(x,s)$ is defined to be the product of $A(x)$ and $A(s)$. $A(x)$ represents the shape of the piezo-actuator when actuated. It is assumed that the piezo creates a uniform cross-sectional variation K over its complete length. The amplitude of this mode as well as the trajectory in time is determined by $A(s)$, though being Laplace transformed. The solution to (11) can be computed straightforwardly. If $A(x,s)$ is replaced by $KA(s)$, the first ordinary differential equation (ODE) of (11) reads as:

$$\frac{\partial}{\partial x}z_1(x,s) + \frac{s}{c_w+v}z_1(x,s) = \frac{-s(c_w-v)}{2(c_w+v)}KA(s) \tag{12}$$

Using the solution at $x=0$, $z_1(0,s)$, as boundary condition, the solution to (12) can be written as:

$$z_1(L,s) = z_1(0,s)e^{\frac{-sL}{c_w+v}} - \frac{KA(s)(c_w-v)}{2}\left(1 - e^{\frac{-sL}{c_w+v}}\right) \tag{13}$$

A similar computation reveals the solution for the second ODE of (11):

$$z_2(0,s) = z_2(L,s)e^{\frac{-sL}{c_w-v}} + \frac{KA(s)(c_w+v)}{2}\left(1 - e^{\frac{-sL}{c_w-v}}\right) \tag{14}$$

The solution to (11) can be written in vector form as:

$$\begin{bmatrix} z_1(L,s) \\ z_2(0,s) \end{bmatrix} = \begin{bmatrix} e^{\frac{-sL}{c_w+v}} & 0 \\ 0 & e^{\frac{-sL}{c_w-v}} \end{bmatrix}\begin{bmatrix} z_1(0,s) \\ z_2(L,s) \end{bmatrix} + \begin{bmatrix} -\frac{(c_w-v)}{2}\left(1 - e^{\frac{-sL}{c_w+v}}\right) \\ \frac{(c_w+v)}{2}\left(1 - e^{\frac{-sL}{c_w-v}}\right) \end{bmatrix}KA(s) \tag{15}$$

Now, (15) represents a twoport system as depicted as in Fig. 3 (block 1). Here, L_{ch}, L_{co}, A_{co}, A_p represent the length of the channel, the length of the connection, its cross-section, and the surface of the piezo bordering the channel, respectively. Note that $v = 0$ since we assumed

that there is no mean flow. As can be seen, the solution admits a nice interpretation as travelling waves. To obtain the original physical states $p(x,s)$ and $\phi(x,s)$, the inverse transformation of (9) can be applied to the states $z_1(x,s)$ and $z_2(x,s)$ (block 3).

For the connection, a similar approach can be used, except that the cross-section remains constant and can be left out of the mass and momentum equations. The solution is depicted in Fig. 3 (block 2). The last subsystem of the acoustic path is the reservoir. For the waves that come from the channel it acts as open end as the reservoir contains a large amount of ink compared to that within an ink channel. In Fig. 3, the reservoir is taken into account (block 4).

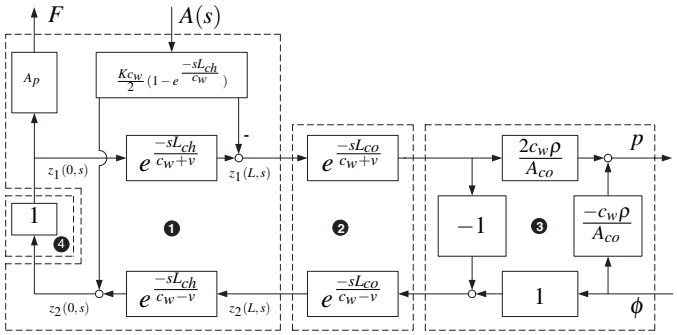

Fig. 3. Graphical interpretation of the acoustic path

C. The fluidic path

The fluidic path consists of the nozzle and droplet formation. However, droplet formation is accounted for slightly differently compared to the other subsystems, since it does not actually make part of an inkjet channel. Droplet formation is computed as postprocessing step according to [6]. On the basis of the meniscus velocity trajectory computed by an inkjet channel model, the droplet properties can be computed. The remainder of the fluidic path, the nozzle, is modeled as an impedance. Note that there are many other options (e.g. [12]).

During the derivation of the nozzle impedance it is assumed that the nozzle is completely filled with ink at all times. Though this assumption is violated in the actual system, the amount of ink is so small that this assumption still holds. Newton's second law for the nozzle, stated in terms of $p(s)$ and $v(s)$, reads as:

$$p(s)A_n = \rho A_n L_n s v(s) + \frac{8\pi\mu L_n}{A_n} v(s) \tag{16}$$

with A_n, L_n, and μ being the nozzle's cross-section, length, and viscosity, respectively. The friction due to the pressure gradient across the nozzle is accounted for in the second term assuming a Poiseuille flow profile. According to the definition, the nozzle impedance can be written as:

$$Z(s) = \frac{p(s)}{v(s)} = \frac{\rho L_n A_n^2 s + 8\pi\mu L_n}{A_n^2} \tag{17}$$

To compute output $\phi(s)$ given the input $p(s)$, we get:

$$\phi(s) = A_n v(s) = A_n \frac{p(s)}{Z(s)} = \frac{A_n^3}{\rho L_n A_n^2 s + 8\pi\mu L_n} \tag{18}$$

In Fig. 4, the fluidic path is depicted (block 5).

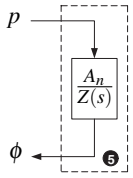

Fig. 4. Graphical interpretation of the fluidic path

D. The actuation

Piezoelectric material acts as a twoport system quite naturally. It becomes electrically polarized when subjected to mechanical strain and strained when subjected to an electric field (e.g. [13]). For the piezoelectric actuator of an inkjet channel, the voltage V of the input pulse and the force F that acts on the piezo surface bordering the inkjet channel are selected as inputs. The electrical charge q measured and the displacement u of the piezo actuator are regarded as outputs. The behavior of the actuator then can be described by the following set of equations:

$$\begin{bmatrix} q \\ u \end{bmatrix} = \begin{bmatrix} C & d \\ d & 1/k \end{bmatrix} \begin{bmatrix} V \\ F \end{bmatrix} \tag{19}$$

with d, k, and C the piezoelectric charge coefficient, the stiffness of the piezo, and the piezo capacity, respectively. The values of these parameters depend on the specific piezo material used. However, their values are highly influenced by the specific structure that surrounds the piezo actuator, such as for example the substrate to which the actuator is attached. To account for these effects, packages like Ansys or Femlab can be invoked to compute the so called effective parameters of the piezo actuator. Irrespective of the complexity of the actuator, as long as the effective parameters can be computed, (19) can be used.

The following remarks are noteworthy. First, note that the fluid-structure interaction is taken into account via the stiffness of the piezo. A displacement of the piezo results via the ink in a force sensed by the piezo. This force on its turn causes a displacement of the piezo via the piezo's stiffness. This way, the fluid-structure accounted for. Second, in this paper it is assumed that the piezo actuator deforms according to its zeroth order mode. However, the approach presented in this paper admits using other modes as well. This can be achieved by using another forcing function $A(x)$ that represents the desired actuation shape. Third, cross-talk

can also be accounted for. Basically, cross-talk results in a change of forcing function as well. This effect can be quantified using for example a FEM package. Accounting for cross-talk is important for the design of the printhead itself as well as for the design of input pulses or controllers. Also, accounting for cross-talk is the key to generate a complete printhead model. Once the cross-talk is known, an array of channels can be used instead of a single one. Finally, as can be seen in Fig. 5, the piezo capacity is left out of the twoport model. In the measurement setup, this piezo is compensated for.

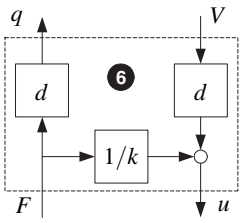

Fig. 5. Graphical interpretation of the actuation path

E. The complete twoport system

In the previous subsections, the subsystems that make up the inkjet channel model have been discussed. To couple the various subsystems, normally one uses a staggered scheme of some kind ([10]). For example, a sequential staggered scheme is depicted in Fig. 6 and comprises the following steps. First, the response of system 1 to a certain input is computed. Second, this response is used as input for system 2. Next, after having computed the response of system 2 to this input, system 1 can be provided with a new input a timestep Δt later. As long as the timestep is kept sufficiently small, this is a valid approach. However, the computational load is very high, especially if more than two systems are to be coupled.

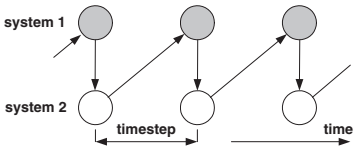

Fig. 6. Sequential staggered solution procedure

For most inkjet printhead models, a computational fluid dynamics package is used to model the behavior of the acoustic and fluidic path and a finite element package for the actuation path. In this paper, only first principle modeling has been used such that analytical expressions are available for the formulation of twoports. One major advantage of the presented approach is that the use of staggered scheme can be avoided. Instead, the Redheffer star product can be used. Given two twoports as depicted in Fig. 7, the coupled system can then be computed according to:

$$\begin{pmatrix} v_1 \\ v_6 \end{pmatrix} = \begin{pmatrix} a_2(1-c_1b_2)^{-1}a_1 & c_2+a_2c_1(1-b_2c_1)^{-1}d_2 \\ b_1+d_1b_2(1-c_1b_2)^{-1}a_1 & d_1(1-b_2c_1)^{-1}d_2 \end{pmatrix} \begin{pmatrix} v_5 \\ v_2 \end{pmatrix} \tag{20}$$

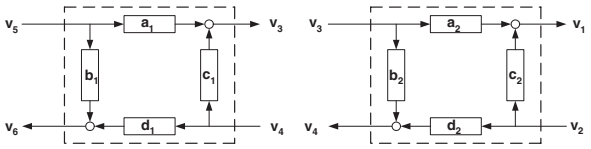

Fig. 7. The coupling of two subsystems using Redheffer's star product

Finally, the resulting overall model is provided with additional viscous damping by shifting its poles away from the imaginary axis without altering their natural frequency. Each resonance frequency can be tuned individually. To analyze the resulting system, the transfer function from a pulse sent to the piezo to the sensor signal measured is taken as measure to compare it to the actual system. In Fig. 8, the theoretically derived inkjet channel model is depicted in gray. In the next section, a further analysis and comparison to the actual system is performed.

IV. EXPERIMENTAL VALIDATION

In this section, the theoretically derived model is compared to the actual system. To that purpose, the frequency response of an inkjet channel is measured using the experimental setup. To identify the frequency response function (FRF) from the piezo used as actuator to the piezo used as sensor, a sine-sweep was used. The amplitude of the sinusoids was chosen such that the inkjet channel was not jetting. The measured FRF includes among other things the piezo amplifier and a low-pass filter with a cut-off frequency of 500 kHz. The latter is used to eliminate the high-frequent piezo behavior. The amplifier and low-pass filter cause a significant phase drop at high frequencies.

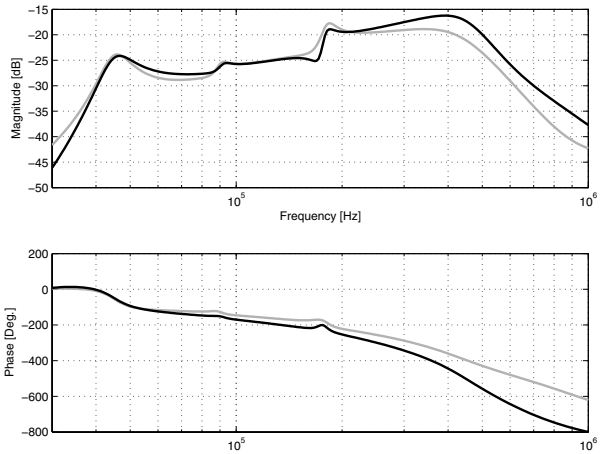

Fig. 8. FRF from the piezo actuator to the piezo sensor; measured (black) and theoretically derived (gray)

To compare the measured and theoretically derived FRF, the low-pass filter is incorporated in the frequency response of the theoretical model as well. Also, since the derivative of the electrical charge is measured instead of the charge itself, a differentiator is added to the theoretical model. In Fig. 8, the resulting theoretical and measured FRF are depicted. Based on Fig. 8, it is concluded that the actual system is modeled accurately. Except for some small differences,

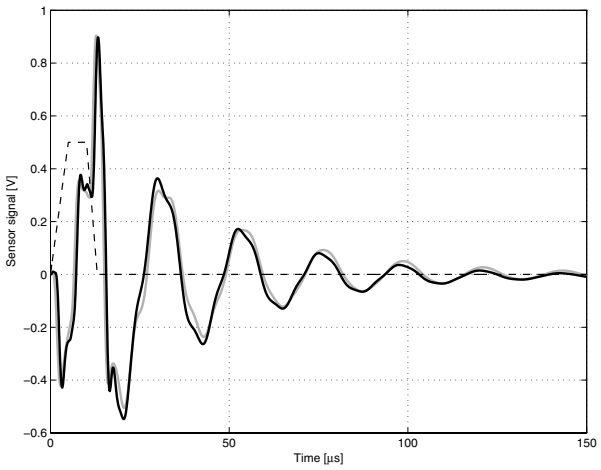

Fig. 9. Sensor signal resulting from a standard trapezoidal pulse (black dotted, scaled); measured (black) and simulated response (gray)

the location and magnitude of the resonance frequencies match. In Fig. 9, the measured and simulated response to a standard trapezoidal actuation pulse are depicted. Despite the fact that this pulse results in a droplet being jetted by the inkjet channel, the measured response is predicted by the theoretical model quite accurately. Altogether, for the control purpose in mind, the theoretically derived model offers an excellent starting point. The remaining model inaccuracies can be handled by ILC quite well.

To improve the current theoretical model, the following refinements can be applied to it. First, the deformation of the actuator $A(x)$ can be modeled more accurately such that it matches the actual deformation of the piezo more closely. Second, the quite coarse model used for the nozzle block can be improved. Note that these refinements are not required for a successful application of ILC, as is demonstrated in section V.

V. ILC CONTROL FOR AN INKJET CHANNEL

In Section II, the functioning of an inkjet channel was explained using the concept of travelling waves. Based on this interpretation, a theoretical model has been derived in Section III that matches the measured FRF of an actual system accurately. Apparently, a relatively simple physical model suffices to that purpose. This model and the physical insight it provides can be now be used for control.

An important issue in inkjet technology is the strive for higher jetting frequencies. As discussed in Section II, inkjet printheads function thanks to resonating fluid-mechanics. At the same time, however, these limit the attainable jetting frequency since the residual vibrations must be damped first prior to jetting a next droplet. Typically, it takes around 200 μs for the pressure waves to be damped such that a next droplet can be jetted: this to guarantee the same droplet properties each time a channel is actuated. Given the highly repetitive character of the jetting process, ILC seems a logical choice as control strategy to accomplish active damping of the fluid-mechanics.

In this paper, use is made of ILC in the lifted setting, see [18], [19]. The accompanying control structure is depicted in Fig. 10. The mapping H is the impulse response matrix of the process sensitivity and S is the sensitivity. In case of the printhead, only open-loop dynamics are present such that H just equals the plant and S the identity. The learning matrix is represented by L and may be non-causal and time-varying. z^{-1} is one trial delay operator and can be seen as memory block. The trial length N equals 1000 corresponding with the sample rate of 10 MHz and the DOD frequency of 10 kHz. Signal u_k is a vector containing the system's inputs or states of the ILC system. Signal y_k is the system output, $\hat{y}_{ref}$ the reference trajectory, and d the disturbance. e_k is the error output. The update of the system's input is Δu_k and u_{k+1} is the input for the next trial $k+1$. At the k-th trial, signal u_k is provided to the system, resulting in the integrated output y_k. The output y_k is then subtracted from the reference y_{ref} to obtain the error e_k. Based on this error, the learning controller computes the adjustments to the input Δu_k that, added to the previous input, forms the input for the next trail u_{k+1}.

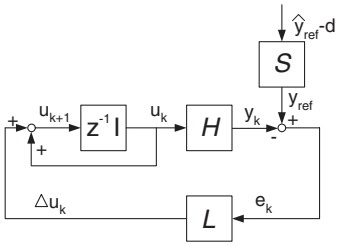

Fig. 10. Lifted ILC control structure in the trial domain

The control goal is to achieve higher jetting frequencies while preserving the droplet's properties. By choosing the current sensor signal as controlled variable, the control goal has to be translated in a suitable reference trajectory for the pressure in the channel. This trajectory now consists of two parts. During the first part, the trajectory is constructed such that a droplet of certain predefined properties results. During the second part of the reference trajectory, the fluid-mechanics is brought to a rest as soon as possible after the firing of a droplet. By doing so, the conditions for higher jetting frequencies are created. To actually construct the reference trajectory the following procedure is adopted. As starting point for the construction of the reference trajectory, the one depicted in Fig. 9 is used. The first part up to the firing of a droplet is left unchanged (up to 20 μs), whereas during the remainder of the time the pressure is forced to a rest by speeding up the damping. The pressure is not forced to a rest immediately but somehow gradually. This is done to ensure the refill of the nozzle with ink and to avoid too high actuation voltages. The resulting reference trajectory is depicted in Fig. 11.

For a detailed description of ILC controller synthesis, one

is referred to [11], [18], [19]. The resulting ILC controller is implemented on the experimental setup. Next to the reference trajectory, the sensor signal resulting from a standard trapezoidal and the learned ILC pulse are shown in Fig. 11. The accompanying actuation pulses are shown in Fig. 12. Based on Fig. 11, the conclusion is drawn that the reference trajectory is attained. As discussed, the first part of reference trajectory up to the firing of a droplet is the same as is realized by the standard trapezoidal pulse. Consequently, it is not surprisingly that the learned ILC pulse resembles the standard trapezoidal pulse for the first part. After that, the ILC controller adjusts the actuation pulse such that the fluid-mechanics follow the desired trajectory. Apparently, the theoretical model is accurate enough to ensure convergence and thus can be used to design input wave forms that enable higher jetting frequencies.

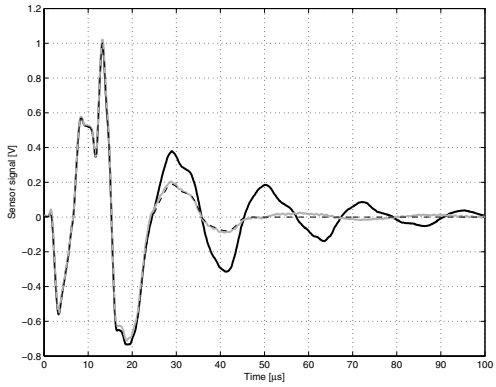

Fig. 11. Sensor signal; without ILC (black), with ILC (gray), and the reference trajectory (black dotted)

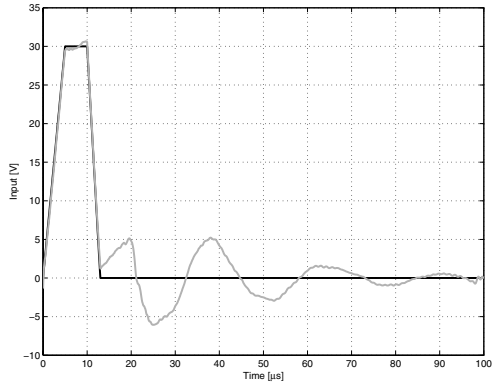

Fig. 12. Actuation signal; standard trapezoidal (black) and ILC pulse (gray)

VI. CONCLUSIONS AND RECOMMENDATIONS

In this paper, an inkjet printhead model has been derived using a series connection of bilaterally coupled multiports. It has been shown that by restricting to first principle modeling only and the use of the Redheffer star product for the coupling of the subsystems, the computational load could be kept low while achieving good accuracy. The resulting model and the physical insight it provides have been employed within an ILC framework to design input wave forms that leave the droplet formation undisturbed while bringing the channel to a rest quickly after droplet ejection. Consequently, a higher jetting frequency can be attained. The successful implementation of ILC based on the obtained model demonstrates the model's applicability to control. Further improvement of the model as well as its use for control is subject to ongoing research.

VII. ACKNOWLEDGMENTS

The authors are grateful to Océ-Technologies B.V. for their support of the research reported here.

REFERENCES

[1] R. Bennett, "Precision Industrial Ink-jet Printing Technology for Full Color PLED display and TFT-LCD manufacturing", *in Proc. of the 3rd International Display Manufacturing Conf.*, Taipei, Japan, 2003.

[2] P.W. Cooley and D.B. Wallace and B.V. Antohe, "Application of Ink-jet Printing Technology to BioMEMS and Microfluidic Systems", *in Proc. SPIE Microfluidics and BioMEMS Conference*, San Francisco, CA, October 2001.

[3] W. Voit et al., Application of inkjet technology for the deposition of magnetic nanoparticles to form micron-scale structures, *IEEE Proc. Science Measurement and Technology*, vol. 150, 2003, pp. 252-256.

[4] H. Wijshoff, Free surface flow and acousto-elastic interaction in piezo inkjet, *Proc. NSTI Nanotechnology Conf. and Trade Show*, vol. 2, pp. 215-218, Boston, MA, 2004.

[5] European Patent 1 378 360 A1

[6] J.F. Dijksman, Hydrodynamics of small tubular pumps, *Journal of Fluid Mechanics*, vol 139, pp. 173-191, 1984.

[7] H. Seitz and J. Heinzl, Modelling of a microfluidic device with piezo-electric actuators, *Journal of Micromechanics and Microengineering*, vol. 14, pp. 1140-1147, 2004.

[8] R.M. Redheffer, On a certain linear fractional transformation, *Journal of Math. and Phys.*, vol. 39, pp. 269-286, 1960.

[9] H.M. Paynter, Analysis and Design of Engineering Systems, *The MIT Press*, Cambridge, MA, 1961.

[10] C.A. Felippa and K.C. Park and C. Farhat, Partitioned Analysis of Coupled Systems, *Computer Methods in Applied Mechanics and Engineering*, vol. 190, issues 24-25, pp. 3247-3270, 2001.

[11] M.B. Groot Wassink and N.J.M. Bosch and O.H. Bosgra and S.H. Koekebakker, Enabling higher jetting frequencies for an inkjet print-head using Iterative Learning Control, *accepted for Conf. Contr. Applications*, Toronto, Canada, 2005.

[12] J.E. Fromm, Numerical Calculations of the Fluid Dynamics of Drop-on-Demand Jets, *IBM Journal of Research and Development*, vol 28, no. 3, pp. 322-333, 1984.

[13] J.W. Waanders, Piezoelectric Ceramics. Properties and applications, Philips Components, Eindhoven, 1991.

[14] D. Karnopp and R.C. Rosenberg, Analysis and Simulation of Multiport Systems. The Graph Approach To Physical System Dynamics, *The MIT Press*, Cambridge, MA, 1968.

[15] F.T. Brown, The Transient Response of Fluid Lines, *Journal of Basic Engineering*, December 1962, pp. 547-553.

[16] F.T. Brown, Step Responses of Liquid Lines with Frequency-Dependent Effects of Viscosity, *Transactions of the ASME*, June 1965, pp. 504-510.

[17] C. van Oosten, O.H. Bosgra, B.G. Dijkstra, Reducing Residual Vibrations through Iterative Learning Control with Application to a Wafer Stage, *in Proc. American Control Conference 2004*, Boston, Ma, 2004.

[18] R. Tousain, E. van der Meché, O.H. Bosgra, Design strategies for iterative learning control based on optimal control, *in Proc. 40th IEEE Conf. on Decision and Control*, pp. 4463-4468, Orlando, December 2001.

[19] B.G. Dijkstra, *Iterative Learning Control with applications to a wafer-stage*, PhD thesis, Delft University of Technoloy, 2004.

[20] K.L. Moore, *Itertive Learning Control for Deterministic Systems*, Advances in Industrial Control. Springer-Verlag, 1993.